Colloids and Surfaces A: Physicochem. Eng. Aspects 492 (2016) 88–99

Contents lists available at ScienceDirect

Colloids and Surfaces A: Physicochemical and Engineering Aspects

journal homepage: www.elsevier.com/locate/colsurfa

Effect of roughness and shape factor on flotation characteristics of glass beads

Behzad Vaziri Hassas[a,*], Hidayet Caliskan[b], Onur Guven[b], Fırat Karakas[c], Mustafa Cinar[b], Mehmet S. Celik[c]

[a] Department of Metallurgical Engineering, College of Mines and Earth Science, University of Utah, 135 South 1460 East, Rm 412, Salt Lake City, Utah 84112, USA
[b] Department of Mining Engineering, Faculty of Engineering, Canakkale Onsekiz Mart University, Canakkale 17000, Turkey
[c] Mineral Processing Engineering, Faculty of Mines, Istanbul Technical University, Maslak, 34469, Turkey

HIGHLIGHTS

- Both roughness and shape factor stimulate the bubble particle attachment.
- Shape factor has an effect in very first milliseconds of attachment.
- Surface roughness strengthens the attachment after it occurred.
- Roughness measurements in AFM should be done via Z-stage abundant method.
- Roughness has significant effect on hydrophobicity and surface properties.

GRAPHICAL ABSTRACT

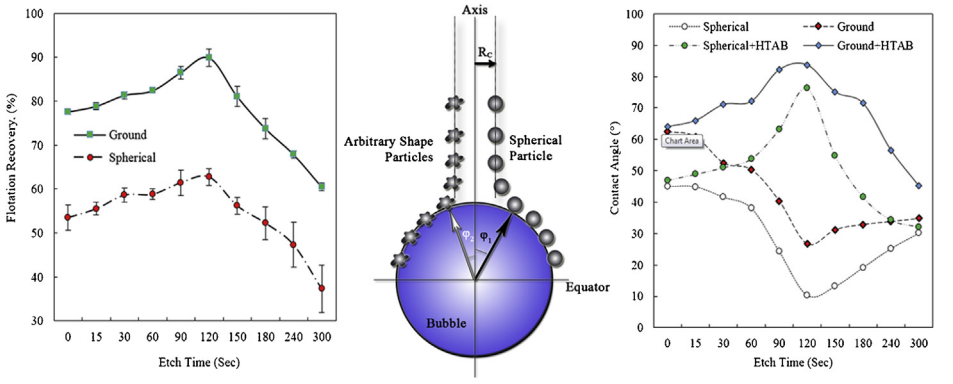

ARTICLE INFO

Article history:
Received 25 September 2015
Received in revised form 5 December 2015
Accepted 20 December 2015
Available online 25 December 2015

Keywords:
Roughness
Shape factor
Flotation
Atomic Force Microscopy (AFM)
Bubble Attachment
Contact angle

ABSTRACT

The effect of surface roughness and shape factor on behavior of particles in flotation has been investigated. Surface roughness of various degrees was applied on spherical glass beads of −150 +106 μm by means of acid etching. The same procedure was also performed on ground glass beads of the same size interval with different shape factors. The effect of these variations on surface morphology of particles was investigated in terms of flotation recovery, contact angle, and bubble-particle attachment. An Atomic Force Microscope (AFM) was used for surface roughness characterizations and a correction methodology on roughness measurements of spherical particles is proposed. A digital image analyzer was used for shape factor characterizations. It is shown that increase in surface roughness improves the flotation recovery, contact angle, and bubble attachment. Shape factor, however, was found to be more predominant in flotation and bubble attachment. This is attributed to the effect of sharp edges of ground particles which triggers the film rupture process and shortens the attachment time.

* Corresponding author at: Metallurgical Engineering Department, 135 S 1460 E, Room 412, William browning Building, University of Utah, Salt lake city, UT 84112, USA. Fax: +1 801 581 4937.
E-mail addresses: behzad.vaziri@utah.edu (B. Vaziri Hassas), hidayet.caliskan@comu.edu.tr (H. Caliskan), oguven@itu.edu.tr (O. Guven), karakasf@itu.edu.tr (F. Karakas), mcinar@comu.edu.tr (M. Cinar), mcelik@itu.edu.tr (M.S. Celik).

http://dx.doi.org/10.1016/j.colsurfa.2015.12.025
0927-7757/

1. Introduction

Colloidal interactions play a crucial role in wide variety of processes particularly in mineral processing. Interfacial and colloidal forces become more significant in some sub-processes that deal with fine and ultrafine particles submerged in water stream such as flotation. Flotation is certainly the most significant, omnibus, and inevitable technique in mineral processing [1]. Surface morphology which includes shape, roughness and crystal structure is one of the most important factors affecting the floatability of particles. Anfruns and Kitchener [2] suggested that the harshness and roughness of the particle stimulates the rupture of the surrounding liquid film in bubble-particle collision increasing the attachment efficiency. Later on Kraskowska and Malysa [3] validated these results by showing that the roughness itself reduces both the induction time and bubble bounce on the surface prior to attachment. Although the effect of shape factor of solid particles in slurry is well known, its influence is generally neglected due to the lack of particle shape characterization methods [4]. The effect of surface morphology on various applications has been also investigated by other researchers [5–10]. Recently Wiese et al. [11], reported that shape factor has also a significant effect on entrainment behavior of particles in flotation. They suggested that it is important to determine a proper milling device and process as it may result in different particle shape in product streams that could affect the amount of entrained particles in further flotation process.

Different grinding methods impart changes in structure, enthalpy, and surface energies of solid particles during wet or dry comminution process leading to morphological changes in particles [12]. Rahimi et al. [13]. showed that particles ground in rod mill produced higher roughness and elongation ratio but lower roundness compared with those ground in ball mill. In addition, contribution of roughness on flotation kinetics was more pronounced than that of shape features. Hicyilmaz et al. [14]. indicated that both talc and quartz minerals ground in a rod mill provided highest flatness and elongation ratio which in turn exhibited higher hydrophobicity. Aside from the type of grinding method, Feng and Aldrich [12] indicated that in dry ground samples, some of milling energy is consumed for crystal defects and these particles have relatively rougher surfaces with a high concentration of microstructural defects which serves as active points to accelerate the reagent adsorption, while the wet ground samples had smoother, cleaner surfaces.

Hicyilmaz et al. [15] reported that autogenous and ball mill produced different shapes. They asserted that the particles having higher axial elongation (higher roundness) showed higher floatability. Ulusoy et al. [16] investigated the floatability of barite and calcite particles having different shapes (roundness) due to different grinding methods namely rod, ball, and autogenous milling. They argued that the particles with higher flatness (lower roundness) showed higher apparent hydrophobicity and better flotation. In their further study, Ulusoy and Yekeler [17] and Hicyilmaz et al. [18]. investigated the surface roughness of barite particles and glass beads along with shape and the overall effect of surface texture on floatability of barite. They concluded that the more elongated (lower roundness) and smoother particles exhibited, the lower critical surface tension and the higher hydrophobicity. These findings are contrary to those reported previously by Hicyilmaz et al. [15]. particularly for the case of barite.

Krasowska and Malysa [3] presented the effect of surface roughness of Teflon plates on the kinetics of bubble attachment. Bubble attachment time was found to be lower for the plates of higher surface roughness, and the bubbles were found to attach during the first collision to rough surface. In another work, flotation of magnetite particles revealed that particles with higher elongation and lower roundness yielded higher flotation kinetics constant [19]. Theoretical model describing colloidal forces operating between a rough particle and a smooth surface suggests that 10–70 nm hydrophobic asperities are capable of significantly reducing surface energy barrier of particle, and could explain accelerated attachment of rough particles to gas bubbles in flotation [20,21].

Above mentioned points show the extent to which both shape factor and surface roughness have impact on mineral process operations especially on flotation processes. It is of significance to understand the mechanism through which these features affect the flotation process.

In this work, the spherical glass beads were roughened through etching and ground to produce different shape factors. Their surface properties and shapes were characterized using atomic force and visual image analysis techniques. The effect of surface roughness and shape factor on contact angle and bubble-particle attachment efficiency both of which identify the success of flotation was elaborated in the light of experimental data.

2. Materials and methods

The Standard safety spherical glass particles used in this study were supplied by Potters Industries. The X-ray fluorescence elemental analysis of the sample show a composition of 61.3% wt. Si, 14.8% wt. Ca, 13.1% wt. Na, 6.0% wt. Al, 3.8% wt. Mg, 1.0% wt. Fe. The washing procedure described by Koh et al. [22], was utilized to remove any dust and chemical contaminants upon producing the desired size fractions and shape factors. Accordingly, all samples were first washed with acid (2.5% v/v H_2SO_4) followed by alkali (2% w/v NaOH) and rinsed with plenty of de-ionized water in between stages and at the end of washing process. All samples were dried and desiccated prior to the experiments. No plasma cleaning was applied in this study as it is reported that the plasma treatment increases the repulsion force between silica particles apparently due to increasing the silicic acid groups upon the surface plasma application [23].

2.1. Roughness and shape factor of particles

Standard glass beads of −800 +90 μm in size were used in experimental studies. The glass beads were first sieved into two main size

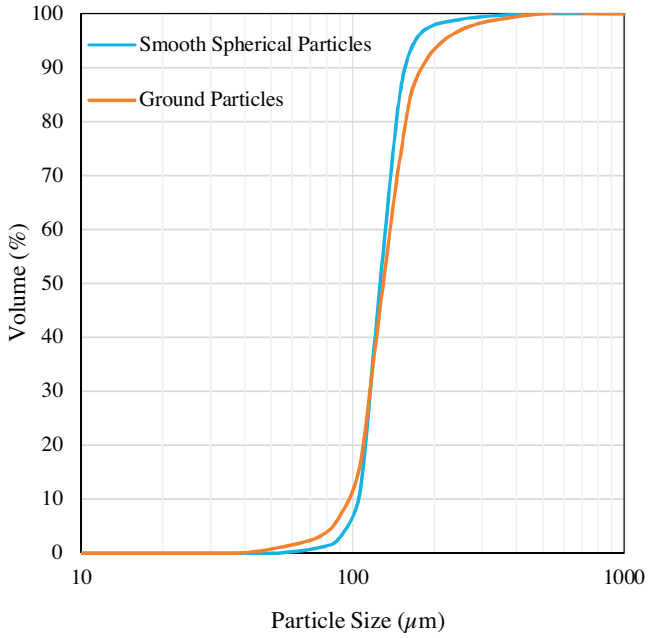

Fig. 1. Particle size distribution of spherical and ground glass bead samples.

Table 1
Shape factor of some known geometries.

Geometry	Roundness
Long rectangle (aspect ratio 10:1)	0.04
Long isosceles (aspect ratio 5:1)	0.23
Triangle (Equilateral)	0.60
Ground particles	0.73
Hexagon	0.86
Ellipse	0.94
Smooth spherical particles	0.97
Circle	1.00

fractions of −800 +150 μm and −150 +106 μm. We will refer to the latter fine particles as "smooth spherical particles". The coarser part (−800 +150 μm) was then ground and sieved again to produce the particle size of −150 +106 μm. These particles will be referred as "ground particles". A ceramic ball mill along with ceramic balls was used in wet grinding for a period of 45 min. Both ceramic mill and balls were cleaned using quartz powder following by ethanol and excessive DI water to prevent any contamination. In order to reduce the influence of particle size on flotation recovery and all other supplementary tests, the size of smooth spherical and ground particles were kept the same. The size measurements of both particle types using Malvern MU-2000 laser particle size analyzer are presented in Fig. 1.

Leica Qwin brand visual particle shape analyzer in which particle's 2D boundaries are selected by the user (Fig. 2) was utilized to measure the shape factor of particles. The roundness of selected geometry was then calculated by the software and reported as number which stands for deviation from a full round circle; in each image analysis run at least 300 particles were selected and processed using the software.

The calculated roundness values of some known geometries with detailed mathematical description given by Ulusoy and Yekeler [17] are presented in Table 1.

In order to induce the required roughness on the surface of particles, 10% w/w Hydro Fluoric (HF) acid 40% Sigma–Aldrich was prepared. Polyethylene labware was used in all steps of etching process. The suspension was stirred using a plastic-coated magnetic bar in a polyethylene beaker for a desired time. Samples were immediately rinsed upon etching with plenty of DI-water to prevent further exposure to acid, dried and kept in a desiccator. It should be mentioned that very strict and appropriate safety precautions were taken during experiments in which HF acid was used. All glassware were replaced with adequate polypropylene equipment. SEM micrographs of different samples with varying magnifications are presented in Fig. 3.

Surface morphology and roughness of the samples were determined by a Park System XE-70 Atomic Force Microscope (AFM) in non-contact mode. The non-contact cantilever Mikromasch NSC-15 purchased from Park System Co., was used. Surface morphology of the plate shape samples is easy to determine by AFM, however, measuring the surface features on the samples with different shapes like spherical particles should be done in a certain way to decrease the possible associated errors as the shape of particle itself has influence on the results. In general, root mean square roughness of the samples is reported in the literature. In this study, in order to increase the accuracy, roughness of the particles is reported as arithmetic average (R_a) and root mean square (R_q). *Ra* and *Rq* are calculated based on Eqs. (1) and (2)

$$R_a = \frac{1}{n}\sum_{i=1}^{n}|y_i| \tag{1}$$

$$R_q = \sqrt{\frac{1}{n}\sum_{i=1}^{n}y_i^2} \tag{2}$$

where n is the number of measured points, y is the height of measured point.

Since the spherical particles of around 100 μm are used in this study, the contact-mode topography method of AFM was found inappropriate for roughness measurements. Variations in the height of the Z-stage of the AFM due to the shape of the sample can affect the results. In this method, roughness of even an atomically smooth sphere will be reported unequal to zero as the mean line will be determined based on the particle shape itself (Fig. 4).

A mean line is calculated by AFM considering all measured points on cantilever path line, once the height of the coordination of measured points on particle surface is reported. Roughness of the surface is calculated based on the difference between the probing path line and average line. Since the produced average line differs from the probing path line, this difference will be reported as roughness with considerable associated error in the data. In order to prevent such error, we used non-contact oscillation method to measure roughness and reported it as both R_a and R_q. In this method, cantilever oscillates in its resonant frequency to have the maximum height of deflection. When the oscillating probe approaches the sample and enters to the force field of its surface, the oscillation changes as a result of interaction between the cantilever and these forces. Dumping of the oscillation of the cantilever leads to a reduction in phase and amplitude of the oscillation. These changes are monitored by transducer and feedback loop changes the Z-stage height of the AFM up to a certain point to match the output and input signals [24]. Fluctuation in amplitude of the oscillation cancels the errors from changes in Z-stage and the outcome is a lateral measurement of the surface (*XY* coordinates) within the Z range of cantilever oscillation. This probing technique is thus believed to be the first applied in roughness evaluation. It should be noted that as a general rule all surface roughness measurements are done in contact mode. Researchers have generally worked on flat surfaces which automatically cancels the Z-stage error.

2.2. Flotation

A micro flotation setup with flotation cell of 150 ml and glass frit for aeration was employed. Nitrogen (N_2) was used as a gas phase in flotation experiments. For each run, 1 g of sample was conditioned for 10 min in 1% wt. stock solution of desired concentration prior to flotation. An automated setup was utilized for flotation with the aim of reducing human errors. Float and sink products were collected after flotation, dried, and weighed to calculate the flotation recoveries. No frother was used in flotation experiments. As a collector, Hexadecyltrimethylammonium bromide (HTAB, CTAB, or Cetrimonium Bromide) purchased from Sigma–Aldrich was used. The pH of the DI water-glass beads suspension system was measured as 6.2 and did not exceed pH 7 in the presence of surfactant.

Flotation recovery in experiments was calculated based on the weight ratio of floated part to feed sample weight as shown in Eq. (3).

$$R\% = \frac{C}{F} \times 100 \tag{3}$$

where R is recovery, C and F are amount of sample floated, and total feed weight, respectively.

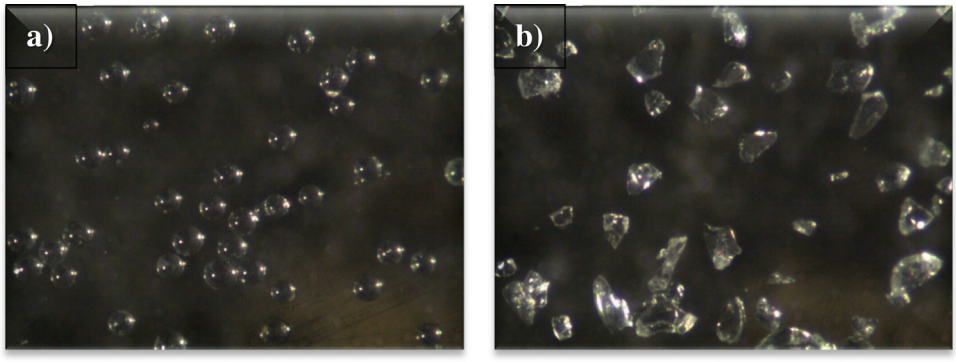

Fig. 2. Image analysis micrographs of (a) spherical, (b) ground particles.

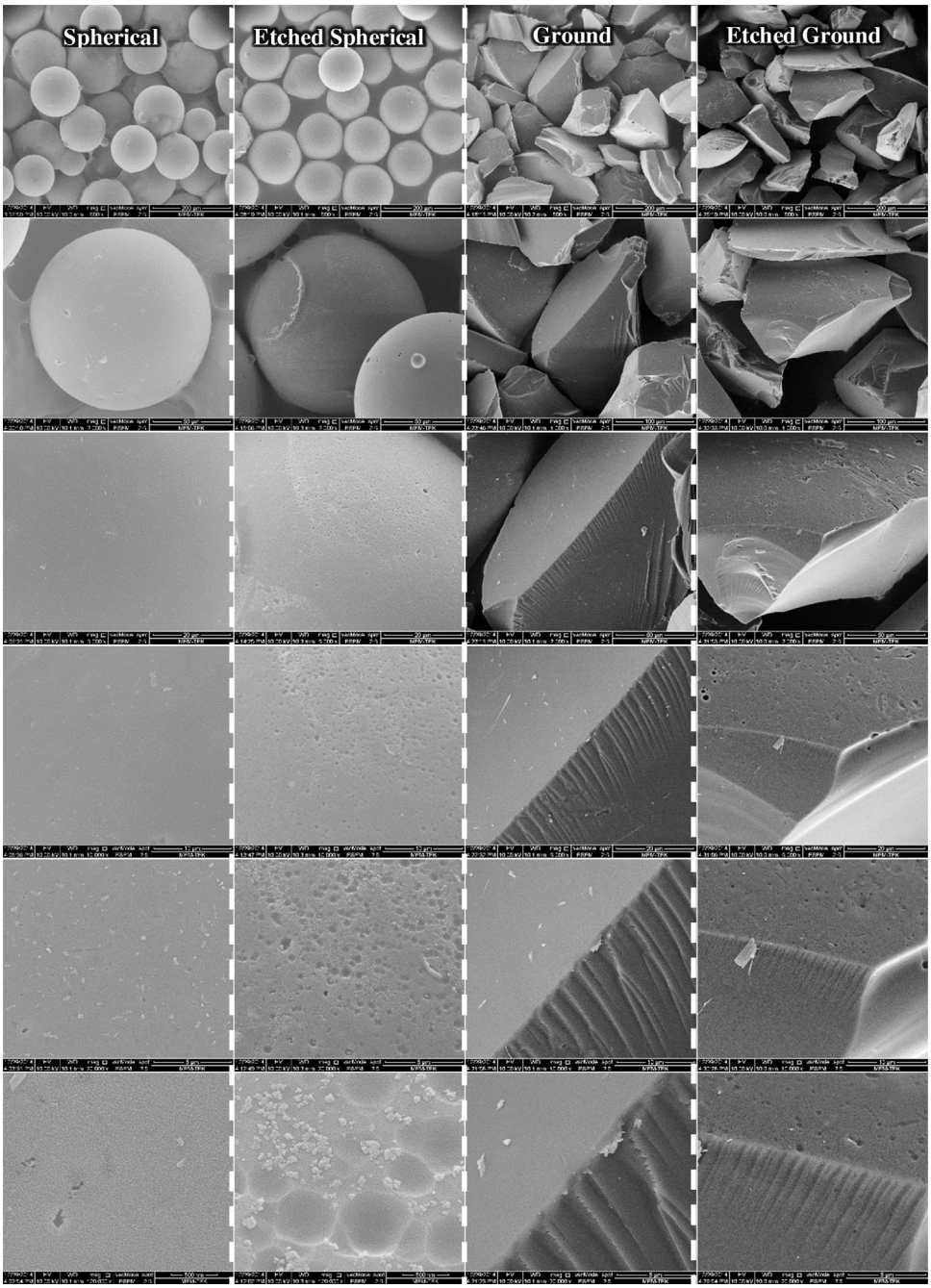

Fig. 3. SEM micrographs of spherical, etched spherical (120 s), Ground, and Etched Ground samples at different magnifications (increasing magnification for each column from up to down).

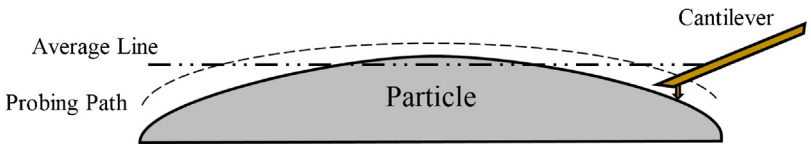

Fig. 4. Schematic representation of AFM tip and its moving path on a spherical particle.

2.3. Contact angle

Various methods for contact angle measurements have been developed for different experimental conditions. Two methods for contact angle measurement of powder samples are suggested, namely, wicking, and powder tensiometry [25]. Although Washburn equation is used for both as a special design, the capillary rise setup was developed for wicking measurements in this study. Discussions and application of wicking method is given in detail elsewhere [26,27]. In this work, Hexane was used as a completely wetting non-polar agent. Constant values in Washburn equation were determined to enable calculation of water contact angle on the sample.

2.4. Bubble attachment efficiency

It is clearly shown that the bubble-particle interaction is the most important sub-process in flotation. Capture efficiency (E_{cap}) or collection efficiency is composed of the probability of three sub-steps as given in Eq. (4) [28–31].

$$E_{cap} = E_c \times E_a \times E_s \tag{4}$$

where E_c, E_a, and E_s are collision, attachment, and stability (detachment) efficiency respectively. A deep understanding of these microprocesses is a fundamentally necessary in predicting rate constant of flotation kinetics [28,32–35].

Collision efficiency (E_C) is statistically defined as the ratio of the number of particles attaching to a bubble, to the number of particles approaching the bubble at a great distance in a flow tube with a cross sectional area equal to the projected area of the bubble (Eq. (5)) [36].

$$E_C = \left(\frac{R_C}{R_b}\right)^2 \tag{5}$$

where R_c and R_b are collision and bubble radii respectively. Collision radius is the distance from bubble centerline, above which particle does not attach to the bubble. Once the collision radius for a particle is below the R_c, this particle hits the bubble, slides on the bubble surface, ruptures the film, and attaches the bubble. The angle at which particle hits the bubble is called grazing trajectory or maximum collision angle (ϕ) above which no attachment may happen (Fig. 5) [37–39]. Attachment of a particle is impossible at the point far from bubble front pole vicinity due to particle rebound on the bubble surface and the higher angle of collision than the angle of tangency [40].

In this study we kept the R_c, R_b, the height of particle release point and in turn the relative velocity of particle-bubble pair constant. In these conditions, we monitored the angle at which a successful attachment is achieved. All these parameters are influenced by micro-hydrodynamic conditions which in turn contingent upon particle size, surface properties and other particle characteristic parameters [41].

Attachment and detachment efficiency also affect the capture efficiency, flotation rate constant (kinetics) and in turn the total flotation recovery [31,42,43]. Both attachment and detachment efficiency can be investigated experimentally. The first experimental technique in determining true flotation kinetics was introduced by Anfruns and Kitchener [2,44], which is used by other researchers as well [28]. In this method, the tracking of a single bubble to capture the very precise collision moment is not possible or at least not easy.

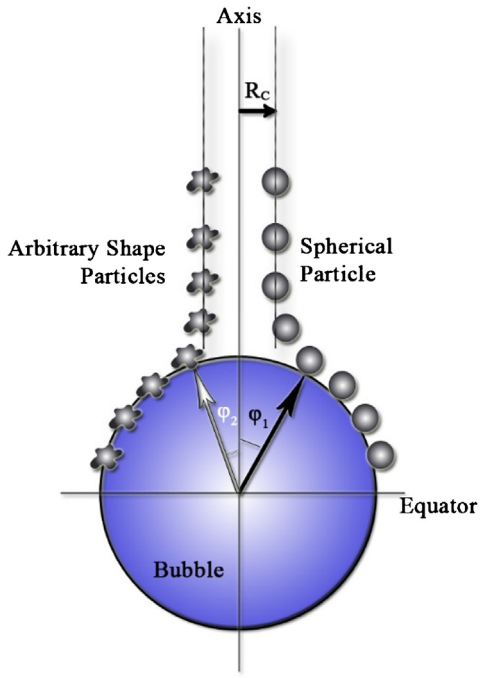

Fig. 5. Schematic representation (not to scale) of bubble particle collision for ground (left) and spherical (right) particles.

A special setup was arranged using high speed video camera to track the particles and measure the attachment efficiency (Fig. 6). A very similar setup with a slight difference in bubble device was used by Verrelli et al. [39,45]. Bubble of 2.5 μL (~1.6 mm in diameter) was produced using a computer controlled digital microsyringe pump. As a bubble dispenser, capillary tube of 1.2 mm of inner and 1.4 mm of outer diameter was used. A Photron512-PCI high speed camera at 4000 frame per second (in 256 × 256 video quality) was used in the experiments. Positions of the bubble dispenser and particle nozzle were fixed in solution tank to clear away the possible errors during experiments. Particle dispenser was located at ~5 mm above the top and ~1 mm from the center of bubble. All bubble attachment experiments were done in 10^{-5} M HTAB solution.

Brabcova et . [41]. used a similar setup supporting the bubble from the bottom, where they found that the liquid flow field is deformed in the presence of capillary supporting the bubble. As the aim of this study is to measure the attachment efficiency, the bubble was supported from one of the sides, letting particles surf on the bubble and stay at the bottom of bubble or detach just under the sway of bubble-particle interaction strength. E_a was then simply calculated as a ratio of number of attached particles to all particles that touch the bubble (Eq. (6)). Both E_c and E_a give the E_{cap}. E_c is explained by grazing trajectory and E_a is calculated by P_{at} equation as follows.

$$P_{at} = \frac{N_{ar}}{N_{cr}} \tag{6}$$

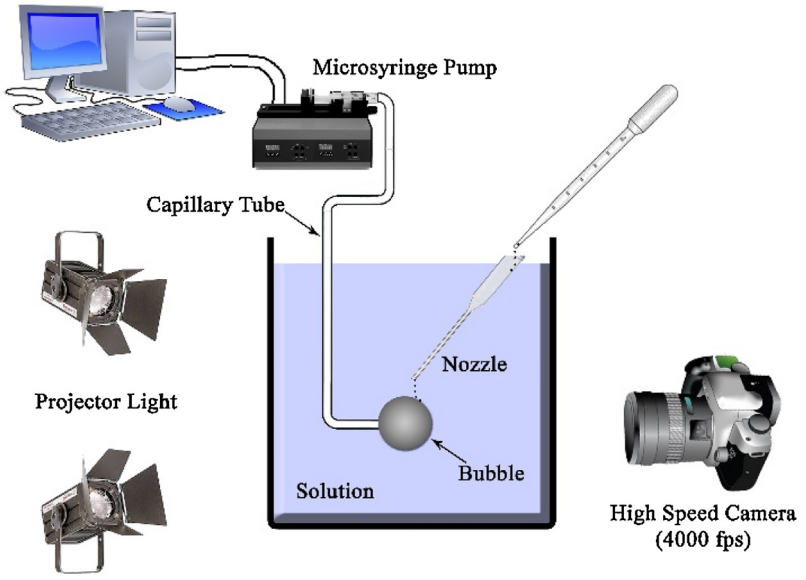

Fig. 6. Experimental set up of Bubble-Particle attachment videography.

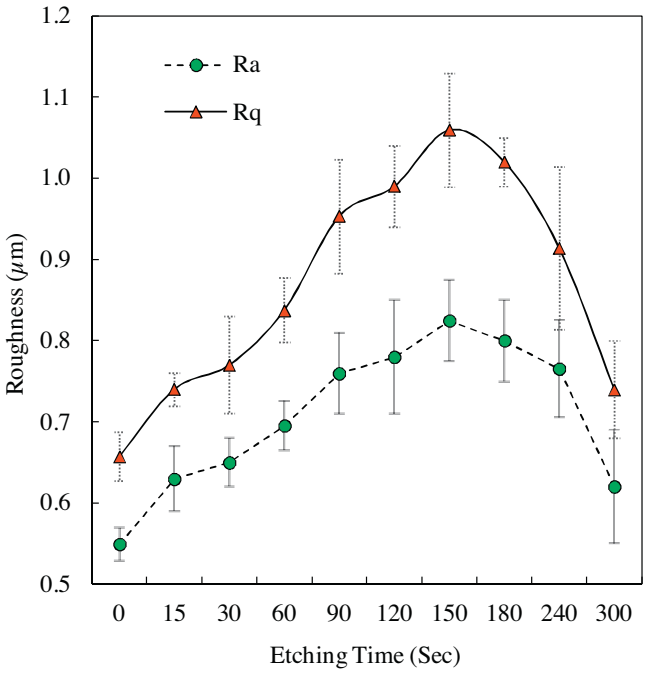

Fig. 7. Arithmetic average (Ra) and root mean square (Rq) roughness values of etched glass beads evaluated by AFM versus etching time.

where P_{at} is the probability of attachment, N_{ar} and N_{cr} are quantity of attached and collided particles in real rates per unit time [34].

2.5. Bubble attachment time

Various methods have been used in previous works in order to measure the induction and attachment time. Comparing alternative experimental methods, Verrelli and Albijanic [46] suggested that in case of using induction timer it is necessary to conduct large enough number of measurements to produce reliable results. They argued the necessity of a calibration method in quantitative reports, which is found not to be vital in case of comparative experiments. In this study, attachment times for different particles are compared and we do not intend to announce any characteristic attachment time for these cases.

In this study BKT-100 Induction Time Test Unit (ITTU) from Bratton Eng. Tech. Assoc. LLC, was used. Induction time values for the glass bead particles with different morphological characteristics were measured. First, the glass bead particles (1 g) were treated in the presence of 100 ml reagent solution for 5 min. Then the suspension was transferred into a small cell under the bubble holder. For induction time experiments, a bubble of ~2 mm in diameter was generated using a micro syringe, and then the distance between the bubble and the bed surface was adjusted using the three-dimensional micro stage adjuster. Bubble was then kept in contact with the bed of particles for a given contact time from 1 to 1000 milliseconds (ms). For each run, it was determined whether attachment occurred or not (1 or 0). Total number of successful attachment was then divided by number of attempts to calculate the probability of attachment. Bubble attachment time was calculated as the time for which 50% of the observations resulted in successful attachment (number of observations with attachment divided by the total number of observations). At least 15 measurements were carried out for determining reliable values at different parts of the particle bed as suggested previous works [46,47]. Attachment of particles to the bubble surface was observed visually through the lens and CCD camera in front of the bubble-holder. The attachment time is determined by the contact at a time at which a pre-selected percentage 50% of the bubble-particle attachment was observed.

3. Results and discussion

3.1. Topography, surface analysis and shape factor

The roughness values of *Ra* and *Rq* obtained from AFM amplitude analyses are presented in Fig. 7 As a function of etching time. For each point 15 different particles were selected on each of which an area of $1 \times 1\ \mu m^2$ was measured for roughness. Error bars on figure show the standard deviation for 15 particles. Fig. 7 shows that both *Ra* and *Rq* of samples increases with increasing etching time up to a certain point (~120–150 s), above which starts to decrease drastically (Fig. 7). It is conceived that above a certain etching time, edges and corners of the particles are affected by acid treatment more than the other surface features. In other

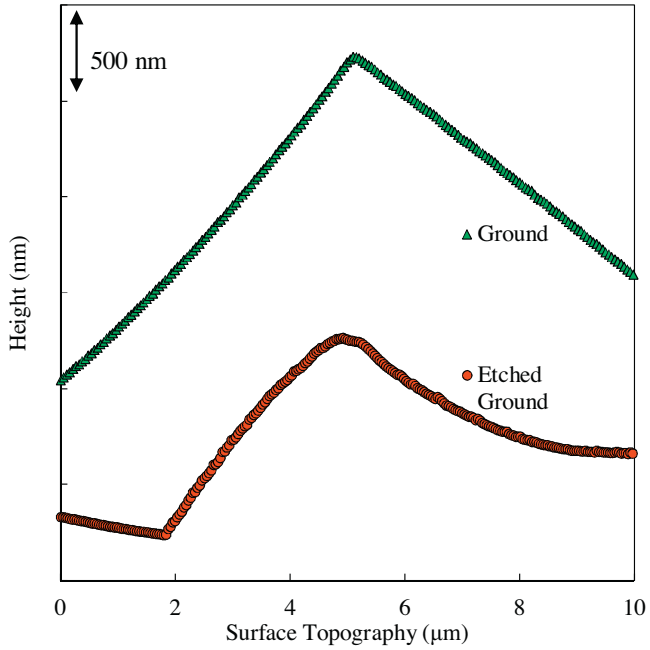

Fig. 8. Surface topography of sharp edge of ground and etched ground particles upon 120 s HF treatment induces soft and round (RED) after etching.

words, scratched and chipped parts of the surfaces start to dissolve in acid faster, as a result, the surface of particles becomes moderately round and smoother upon long etching times. Bibi et al. [48], reported that illite particles after exposure to acid and partial dissolution acquired predominantly sharp edges, with more rounded borders. An early rapid dissolution of illite was ascribed to different factors including fast dissolution of high energy surface sites and the presence of tense surfaces formed during grinding [48].

Solubility and mass transfer strongly depend on the surface free energy of the particle. It is well known that the surface free energy is not uniform on different parts of the surface of a given geometry. Consequently the solubility and mass transfer of a plane face, edge and corner of this geometry differ from each other. Mutaftschiev [49] proposed a calculation methodology for this energy variation based on Born and Stern approaches considering a cubic block of crystal with the given dimensions. The surface energy of the edges was shown to be equal to the half of the work needed to separate two blocks that are connected to each other through a unit length of cube. Mutaftschiev [49] concluded that the crystal lattices become weaken in the vicinity of edges and corners. This phenomenon explains how sharp edges and corners have higher surface potential and in turn higher solubility in acid. This higher solubility causes a decrease in roughness and sharpness of edges of the particles, as shown in Figs. 8 and 9. Topology analysis of single sharp edge of ground particles before and after etching verifies this approach. As shown in Fig. 8, it is the sharp broken edge of ground glass beads becoming smoother after being exposed to HF acid for 120 s (Fig. 8); the sharp edged particles become soft and round.

The same approach is valid for smooth surfaces when they are exposed to acid. As described previously, the roughness of particles decreases after 150 s. Visual topographic analyses of the samples using AFM (Fig. 9) also validate the roughness measurements and this critical inflection point.

3.2. Flotation

Flotation experiments were carried out to observe any improvement in recoveries. The collector dosage was selected at moderate recovery levels such that any increase or decrease upon etching would be visible. In this context, the air flow rate of 60 cm^3/min was kept at medium level to prevent any entrainment due to air bubble flux. Flotation recoveries at different flow rates increase up to a certain HTAB concentration after which slows down. This behavior was already reported [50] and explained on the basis of HTAB molecules forming a bilayer on the particle surface rendering it more hydrophilic. Such behavior is reported both in flotation and dewatering research as both surfactants are used to make the surface of particles hydrophobic [51]. This behavior was investigated in detail by Vidyadhar et al. [52]. on quartz flotation using amine surfactants of different carbon chain length. They showed that for each surfactant and its carbon chain length there is a characteristic concentration and hydrophobicity after which flotation recovery decreases. The concentration of 10^{-4} M was reported for Cetrimonium bromide (HTAB) in agreement with our experiments, as shown in Fig. 10. HTAB concentration of 10^{-5} M was selected for further use in the rest of study.

Flotation recovery of both spherical and ground particles versus etching time is plotted in Fig. 11. Each point in this figure is the average of 5 runs and error bars stand for standard deviation for these 5 experiments. The results are in accord with the trend reported in topography measurements in Fig. 7. Flotation recovery for both spherical and ground particles increases with increasing etching time (or roughness) up to 120 s, after which falls below the initial values of smooth spherical particles. Another significant point in flotation experiments is that the ground particles have higher flotation recoveries compared to spherical ones under all conditions. This result coincides well with those reported in the previous works [22]. It was also found that the statistical variance for flotation recoveries of different roughness levels for ground particles is less than that of spherical particles in the same conditions (Fig. 11). This can be due to the higher detachment rate of spherical particles from the bubble surface. Roughness can also increase the hydrophobic interaction since the probability of trapped gas (nano-bubbles) in the cavities is higher [3].

3.3. Contact angle

Fig. 12 presents that the contact angle of both ground and spherical particles in the absence of a surfactant (HTAB) decreases up to a point (120 s etched) after which it increases again. Contact angle

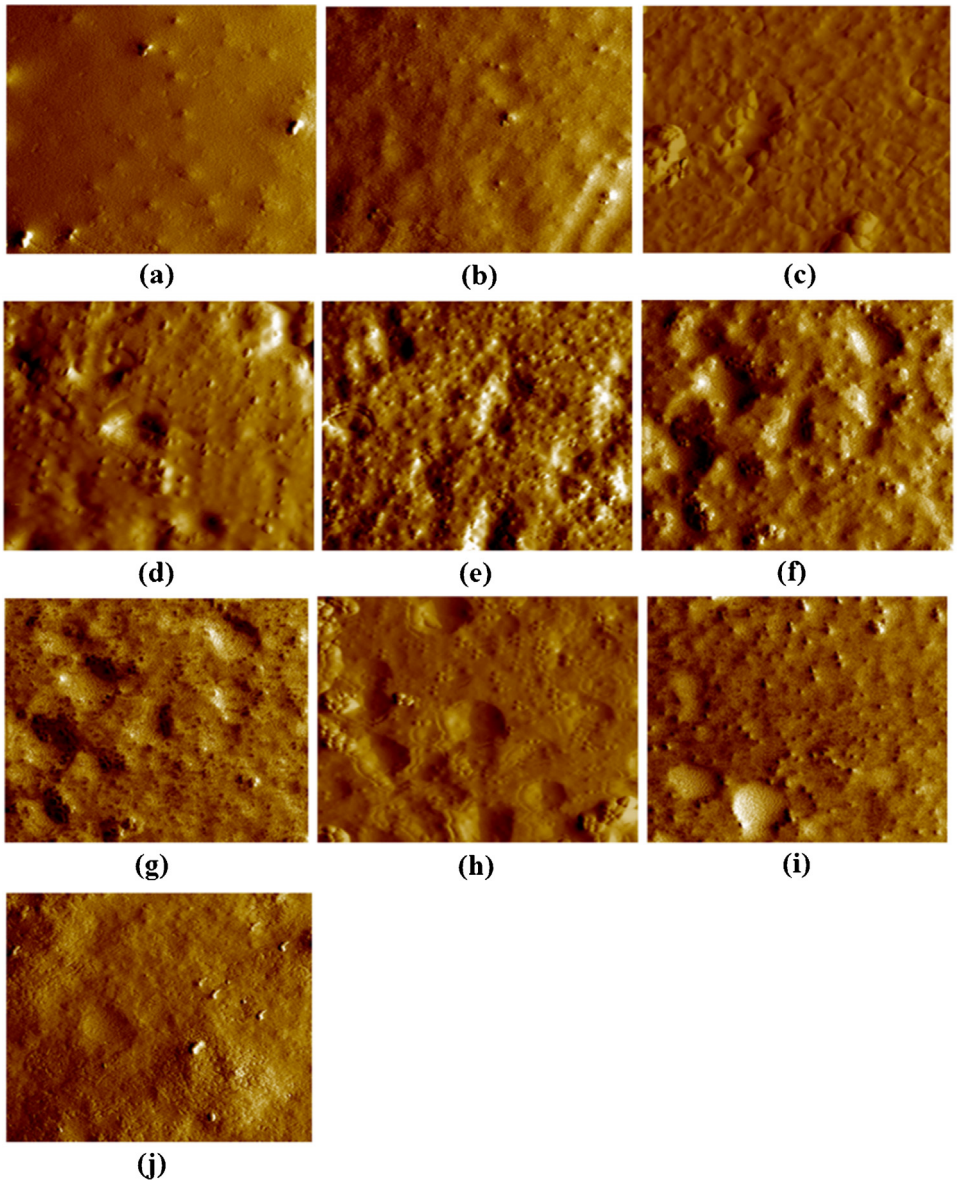

Fig. 9. Selected AFM surface topography (1 μm × 1 μm area) of etched spherical particles vs. different etching times (min): (a) 0, (b) 15, (c) 30, (d) 60, (e) 90, (f) 120, (g) 150, (h) 180, (i) 240, (j) 300.

of the same samples after treatment with 10^{-5} M HTAB for 10 min showed exactly the opposite behavior. Contact angle of hydrophobized samples increases up to the same point (120 s etched) and starts to decrease above that (Fig. 12). It should be emphasized that the contact angles measured in wicking methods corresponds to the advancing contact angle of water on the sample. It is of significant to mention that the contact angle trends are exactly the same as the surface roughness values and flotation recoveries given in Figs. 7 and 11. In both experiments, the maximum etching time of 300 s shows lower values for both contact angle and flotation recovery compared to non-etched smooth spherical particles (Figs. 11 and 12). Effect of roughness for both hydrophobic and hydrophilic surfaces on contact angle has been investigated by various researchers. Wetting properties of rough surfaces can be defined in two models, the Wenzel model and the Cassie-Baxter. Wenzel argued that in a real surface tension of a drop liquid multiplied by cosine of the equilibrium contact angle equals to the *rA* rather than *A* where *A* is the adhesion tension and *r* is defined as the ratio of actual surface to the geometric surface [53]. From this definition it is clear that by increasing roughness, the ratio of actual surface to the geometric surface increases which in turn results in higher contact angle in hydrophobic surfaces, as well as lower contact angle in hydrophilic surfaces. Cassie-Baxter introduced another factor of "porosity" which also has an effect on apparent contact angle without which the equation reduces to the Wenzel approach. Utilization of the porosity factor in Cassie-Baxter approach introduces the interfacial interaction of liquid and its vapor which is trapped on solid surface under the drop due to roughness [54,55].

Although Gao and McCarthy [56,57], criticizes the accuracy of the two approaches, they didn't comment on any other experimental methods such as wicking, immerse heat, etc. Experimental results of this study, however, coincides well with these theories considering the increase in contact area.

Busscher et al. [58], investigated the contact angle and its hysteresis on 12 polymers of different surface roughness. They described effective surface roughness as $R_a > 100$ nm and concluded that the average roughness higher than 100 nm increases the contact angle of those surfaces having contact angles higher than 86°

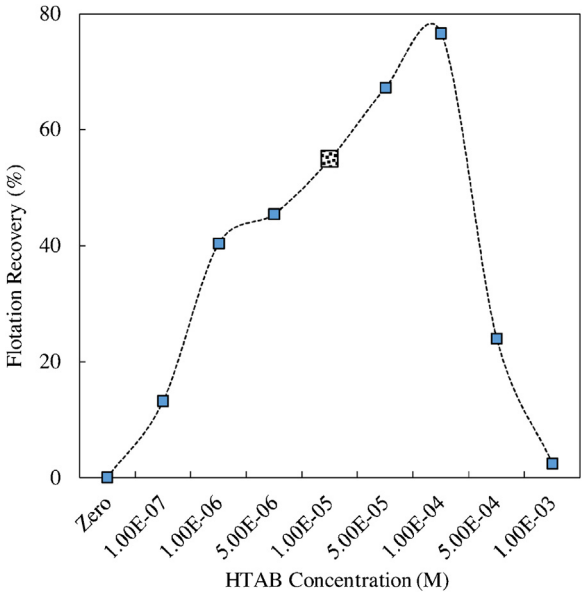

Fig. 10. Flotation recovery of smooth spherical glass beads at 60 cm^3/min gas rate versus various HTAB concentrations—Selected concentration for further experiments is indicated by different marker at 10–5 M.

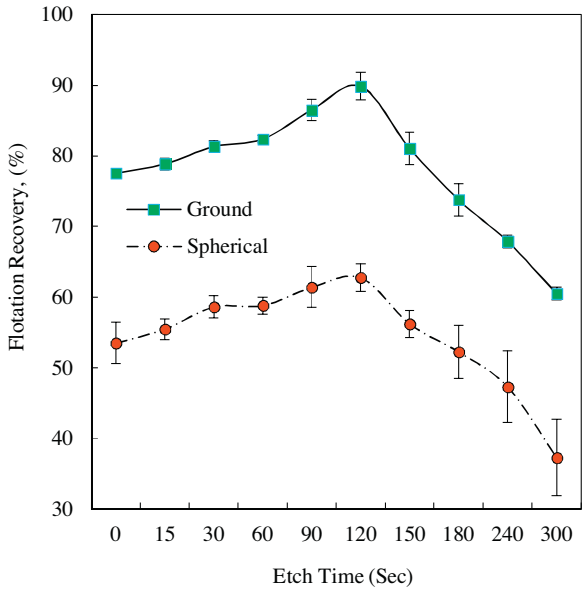

Fig. 11. Flotation recovery of ground and spherical glass beads in 10–5 M HTAB versus different etching time (roughness).

(relatively hydrophobic surface) and decreases the contact angle on the surfaces having the contact angle of below 60° (relatively hydrophilic surface). They asserted that the roughness has no effect on surfaces with contact angle in the range of 60–86°. Chau et al. [59]. reported the results of a previous work done by Johnson and Dettre [60] in which the advancing contact angle of water on wax (naturally hydrophobic) surface increased with increasing surface roughness. Miller et al. [61]. investigated the roughness of vacuum-coated polytetrafluoroethylene (PTFE) using AFM. They concluded that even nanometer surface roughness (~80 nm) strongly affects the wettability of surface. Dang-Vu et al. [62]. studied the effect of roughness on contact angle of glass beads by wicking method and found that the kinetics of rising and penetrating liquids in bed of roughened particles increased by over two fold. They, however, stated that the contact angle does not change significantly.

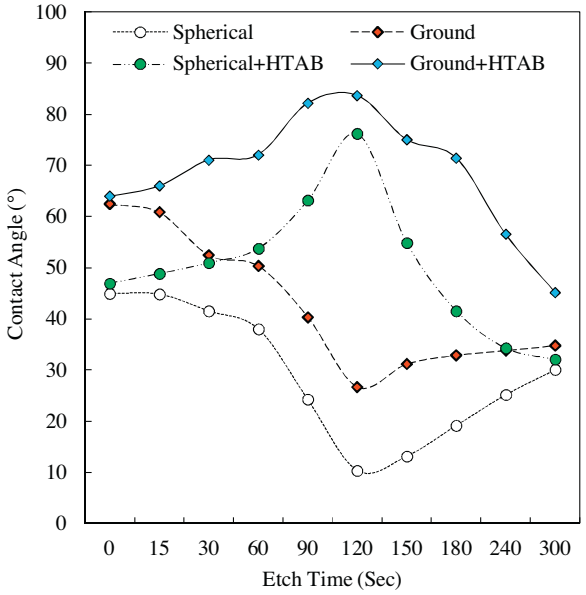

Fig. 12. Advancing water contact angles on ground and spherical particles with and without HTAB pretreatment versus etching time.

This work did not explain the reason for such increase in penetration rate of liquids on roughened bed. Drelich et al. [63]. listed those phenomena affecting the contact angle on rough surfaces as: (i) contortion of the triple point and contact line of three-phases, (ii) distortion of liquid movement due to mechanical and surface free energy barriers of rough surface, and (iii) entrapment of gas between surface features of rough hydrophobic surface which is referred as "nano-bubbles" in various studies [64,65].

3.4. Bubble attachment efficiency

Both grazing trajectory and attachment efficiencies were measured and calculated by high speed videography taken during the experiments. Three cases were selected to represent smooth spherical particles, roughened spherical particles, and ground particles. 25 particles for each case were tracked and average value for grazing trajectory is reported in Fig. 13. In case of attachment efficiency, proportion of number of particles those hit and attached to the bubble was divided by total number of particles hit the bubble surface. Error bars in Fig. 13 show the standard deviation in each point. For rough particles, 120 s etched sample was selected since it was previously found to be the inflection point in flotation and contact angle experiments. It should be mentioned that the bubble surface in this study should be considered as semi-mobile in stokes flow regime. Verrelli et al. [45]. compared the velocity of particles on a stationary bubble with particle velocity prediction on both mobile and immobile bubble surfaces and found the experimental data to represent the intermediate case, as the experimental data fell between mobile and immobile velocity gradients on bubble surface. As shown in Fig. 13, the attachment efficiency of ground particles was found to be the highest among all samples. It is clear that although attachment of rough particles is less than the ground particles, it is considerably higher than that of smooth particles. On the other hand, grazing trajectory, opposite to attachment efficiency, decreases from smooth spherical to rough particles. This indicates that ground particles with their lowest maximum collision angle (ϕ) and highest attachment efficiency acquire the maximum interaction with bubble ($\phi_2 < \phi_1$ as represented schematically in Fig. 5). These results correlate well with the previous studies done on both flotation rate constants and bubble-particle attachment efficiencies

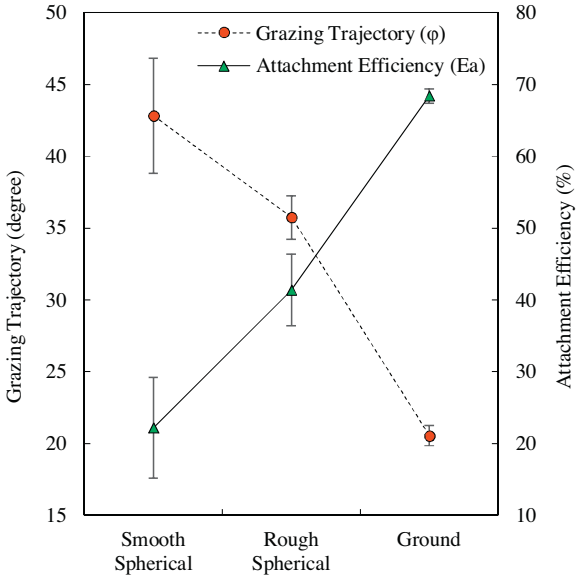

Fig. 13. Grazing trajectory and attachment efficiency of smooth spherical, rough spherical (120 s etch), ground,and rough ground (120 s etch) particles.

[3,9,20,21,39,66]. High speed videography (attached videos) clearly reveals that, once a ground angular particle approaches the bubble surface, it attaches to the bubble by its most feasible position with a quick turn (Video 1). Generally, sliding of ground particles on the bubble surface was not observed before the particle ruptures the film and attaches to the bubble. This quick rupture of bubble film and the attachment process of particle was detected for both ground and rough particles while that for rough particles occurred after a short sliding (Video 2 and 3). Similar high speed camera results were reported by Verrelli et al. [45], but without explanatory comments.

Kouachi et al. [38]. theoretically calculated the attachment efficiency for spherical quartz particles and reported E_a as 30% for particle diameter of 100 μm and bubble velocity of 16 cm/s which is in fair agreement with those reported in this study. It should be emphasized that this actually relative bubble-particle pair velocity. Particle-bubble pairs have been demonstrated to detach themselves easier than the prismatic ones [15]. Gul [67] also reported that the zircon particles having tetragonal crystals (with many angular points) floated first, whereas the heavily abraded ones floated slower. It is also mentioned that the attachment efficiency increases with decreasing bubble velocity [38]. Most of the attachment efficiency models are based on this principle that if the sliding time of the particle is equal to or longer than the induction time the particle attaches to the bubble surface [34,68,69]. Since the angle of grazing (maximum angle of contact) decreases from smooth to rough and to ground samples sequentially, particles get more time to slide on the bubble until equatorial line of the bubble. Consequently, a sliding particle have more chance of rupturing the bubble film and attachment. The results found in our experiments are in good agreement with the previous works as it is reported that roughness and surface asperities have significant effect on bubble-particle attachment and stimulate the bubble film rupture [2], which in turns results in lower attachment time [3].

3.5. Bubble attachment time

Since the effect of particle morphology was determined in terms of flotation recovery, contact angle, and bubble attachment efficiency, evaluation of bubble-particle attachment time will provide a different approach for supporting these findings. In this study, bubble-particle attachment time measurements were conducted for both spherical and ground particles under relatively similar conditions. Of these, the number of samples was reduced to five etching times (0, 60, 120, 240, and 360 s.) for both spherical and ground particles so as to show the effect of both roughness and various shape factors on the above variables.

Table 2
The induction times for spherical and ground particles.

	Spherical	Ground
Etching time (S)	Induction time (ms)	
0	15.1	8.0
60	10.5	9.1
120	7.9	10.8
240	8.3	10.9
360	8.5	11.2

The results of induction times are shown in Table 2. As it can be seen, the longest induction time of 15.1 ms was obtained for smooth spherical particles. This shows that, the tendency for interaction between bubble and particle is low in the case of smooth particles compared to rougher or non-spherical particles. The required time for roughened (120 secetched) spherical particles to attach to the bubble was found as 7.9 ms. Considering these results, it is clear that increasing the roughness of spherical particles resulted in almost twice lower induction times in bubble-particle attachment. A similar trend was also obtained by Zawala et al. [70]; while the induction time range for rough fluorite surfaces was 5–35 ms, it was 200 ms for smooth surfaces. The authors attributed their findings to first the presence of pillars on hydrophobic rough surfaces which led to a greater probability of film rupture as the critical thickness of the wetting film was locally lower on rough surfaces. The second was the presence of entrapped air (nano- or micro-bubbles) on rough surfaces which then facilitated the liquid film rupture.

The measurements for ground particles, however, showed that not only attachment efficiency (as discussed in previous section), but also induction times are governed by the effects of shape factors. Therefore, decreasing angularity by etching of ground particles increased the induction time from 8.0 to 11.2 ms. In the case of spherical particles, induction time was found to reach a minimum at the etching time of 120 s which corresponds to the highest roughness. As mentioned in the previous sections, particle-bubble pairs have been demonstrated to be more likely to detach in the case of round particles [15]. It is clear that angularity plays an important role on both flotation recoveries and induction times; however, the effect of roughness at its maximum peak was found to roughly follow the curve of particle shape.

Various studies in the literature have adapted different methods to determine the bubble-particle attachment time in different particulate or surface systems [3,46,47,71–73]; however, the effect of roughness and shape factor in particular was not investigated in details.

These results further demonstrate the effect of morphological characteristics on flotation recovery and bubble-particle attachment time for glass bead particles. Thus, while etching of spherical particles improves induction times, modification of shape factor through etching of angular particles deteriorates attachment times.

4. Conclusions

The effect of both roughness and shape factor of particles on surface properties and flotation characteristics of glass beads were studied. Both features were found to induce beneficial and adverse effects on flotation sub-processes. A new and corrected roughness measurement method for spherical particles has been introduced using AFM. Roughness calculation based on topograph-

ical height measurements contains considerable associating error as the essence of collected data embraces the spatial coordination of surface itself which has different heights in various points. The finer the particle size, the higher the associated error is. In order to eliminate this error, roughness measurements on spherical particles should be carried out using the proper "amplitude method" which is Z-stage abundant.

Advancing contact angle of water on spherical glass beads, measured via wicking method, was found to decrease by increasing roughness. This trend was found to be vice versa in case of hydrophobized particles where contact angle was found to be higher in rougher hydrophobic particles. Moreover, ground particles were found to follow the same trend with a higher contact angle for all points. These results obey the theoretical approaches of previous works.

Ground particles during flotation were found to recover more efficiently. This reveals that the effect of sharp edges on the particles (shape factor) in flotation. Sharp edges stimulate the film rupture around the bubble at the very first moments of attachment. Bubble attachment efficiency and attachment time outcomes corroborated flotation results in that particle shape particularly is pronounced in the first steps of bubble-particle collision (0–10 ms). Roughness, however, seems to strengthen the existing bubble-particle interactions after induction occurs. Particles with higher roughness were found to have stronger bubble-particle pairs as detachment of these particles was lower than that of smooth particles.

Grazing trajectory for rough particles was found to be lower than the smooth particles. The least grazing trajectory, however, was found for ground particles. This value has a significant effect on particle bubble interaction and attachment. Consequently, attachment efficiency of ground glass beads was revealed to be highest among all. Attachment efficiency was determined to be halved when it comes to rough spherical particles, while it was the lowest for smooth spherical particles among all.

As an overall conclusion it can be asserted that the roughness affects particle's interaction with the surrounding media, while the effect of shape is more related to the micro-hydrodynamic properties of the particle.

Appendix A. Supplementary data

Supplementary data associated with this article can be found, in the online version, at http://dx.doi.org/10.1016/j.colsurfa.2015.12.025.

References

[1] B.A. Wills, Wills' Mineral Processing Technology, Butterworth Heinemann, UK, 2015, ISBN 978-0-750-2006 64450-64451.
[2] J.F., Anfruns, J.A., Kitchener, 1977, Rate of capture of small particles in flotation, Transactions of the Institute of Mining and Metallurgy, Section C: Mineral Processing & Extractive Metallurgy 1977, 86, 9–15.
[3] M. Krasowska, K. Malysa, Kinetics of bubble collision and attachment to hydrophobic solids: effect of surface roughness, Int. J. Miner. Proc. 81 (2007) 205–216, http://dx.doi.org/10.1016/j.minpro.2006.05.003.
[4] M. Oja, R. Tuunila, The influence of comminution method to particle shape, in: Proceedings of The XXI International Mineral Processing Congress, Rome-Italy, July 2000, Volume C, pp. 64–70, 2000.
[5] U. Ulusoy, M. Yekeler, C. Hicyilmaz, Determination of the shape, morphological and wettability properties of quartz and their correlations, Miner. Eng. 16 (2003) 951–964, http://dx.doi.org/10.1016/j.mineng.2003.07.002.
[6] P. Pourgharamani, E. Forssberg, Review of applied particle shape description and produced particle shapes in grinding environments. Part 1: particle shape descriptor, Miner. Proc. Extr. Metall. Rev. 26 (2005) 145–166, http://dx.doi.org/10.1080/08827500590912095.
[7] T.G. Vizcarra, S.L. Harmer, E.M. Wightman, N.W. Johnson, E.V. Manlapig, The influence of particle shape properties and associated surface chemistry on the flotation kinetics of chalcopyrite, Miner. Eng. 24 (2011) 807–816, http://dx.doi.org/10.1016/j.mineng.2011.02.019.
[8] O. Guven, O. Ozdemir, I.E. Karaagaclıoglu, M.S. Celik, Surface morphologies and floatability of sand-blasted quartz particles, Miner. Eng. 70 (2015) 1–7, http://dx.doi.org/10.1016/j.mineng.2014.08.007.
[9] H., Calıskan, B., Vaziri Hassas, M., Cınar, M.S., Celik, 2015, effect of roughness and shape factor on flotation recoveries of glass beads, XVI Balkan Mineral Processing Congress, 17–19 June 2015, Belgrade—Serbia.
[10] V.B. Svetovoy, G. Palasantzas, Influence of surface roughness on dispersion forces, Adv. Colloid Interface Sci. 216 (2015) 1–19, http://dx.doi.org/10.1016/j.cis.2014.11.001.
[11] J. Wiese, M. Becker, G. Yorath, C. O'Connor, An investigation into the relationship between particle shape and entrainment, Miner. Eng. 83 (2015) 211–216, http://dx.doi.org/10.1016/j.mineng.2015.09.012.
[12] D. Feng, C. Aldrich, A comparison of the flotation of ore from the Merensky Reef after wet and dry grinding, Int. J. Miner. Proc. 60 (2000) 115–129, http://dx.doi.org/10.1016/s0301-7516(00) 00010-7.
[13] M. Rahimi, F. Dehghani, B. Rezai, M.R. Aslani, Influence of the roughness and shape of quartz particles on their flotation kinetics, Int. J. Miner. Metall. Mater. 19 (No. 4) (2012) 284–289, http://dx.doi.org/10.1007/s12613-012-0552-z.
[14] C. Hicyilmaz, U. Ulusoy, M. Yekeler, Effects of the shape properties of talc and quartz particles on the wettability based separation processes, Appl. Surf. Sci. 233 (2004) 204–212, http://dx.doi.org/10.1016/j.apsusc.2004.03.209.
[15] C. Hicyilmaz, S. Bilgen, U. Atalay, U. Ulusoy, Effect of particle shape characteristics of particles on flotation, Physicochem. Prob. Miner. Process. 29 (1995) 31–38.
[16] U. Ulusoy, C. Hicyilmaz, M. Yekeler, Role of shape properties of calcite and barite particles on apparent hydrophobicity, Chem. Eng. Process. 43 (2004) 1047–1053, http://dx.doi.org/10.1016/j.cep.2003.10.003.
[17] U. Ulusoy, M. Yekeler, Flotability of barite particles with different shape and roughness, Ind. J. Chem. Technol. 14 (2007) 616–625.
[18] C. Hicyilmaz, U. Ulusoy, S. Bilgen, M. Yekeler, Flotation responses to the morphological properties of particles measured with three-dimensional approach, Int. J. Miner. Process. 75 (2005) 229–236, http://dx.doi.org/10.1016/j.minpro.2004.08.019.
[19] F. Dehghani, M. Rahimi, B. Rezai, Influence of particle shape on the flotation of magnetite, alone and in the presence of quartz particles, J. South. Afr. Inst. Min. Metall. 113 (2013) 905–911, ISSN 0038-223X.
[20] J.W. Drelich, P.K. Bowen, Hydrophobic nano-asperities in control of energy barriers during particle-surface interactions, Surf. Innov. (2015), http://dx.doi.org/10.1680/si.15.00003.
[21] O. Guven, M.S. Celik, J.W. Drelich, Flotation of methylated roughened glass particles and analysis of particle-bubble energy barriers, Miner. Eng. 79 (2015) 125–132, http://dx.doi.org/10.1016/j.mineng.2015.06.003.
[22] P.T.L. Koh, F.P. Hao, L.K. Smith, T.T. Chau, W.J. Bruckard, The effect of particle shape and hydrophobicity in flotation, Int. J. Miner. Process. 93 (2009) 128–134, http://dx.doi.org/10.1016/j.minpro.2009.07.007.
[23] W.R. Bowen, N. Hilal, R.W. Lovitt, C.J. Wright, An atomic force microscopy study of the adhesion of a silica sphere to a silica surface effects of surface cleaning, Colloids Surf. A: Physicochem. Eng. Aspects 157 (1999) 117–125.
[24] P. Eaton, P. West, Atomic Force Microscopy, Oxford University Press Inc., New York, 2010, ISBN: 978-0-19-957045-4.
[25] H.Y. Erbil, Surface Chemistry of Solid and Liquid Interfaces, Blackwell Publishing Ltd., Oxford, UK, 2006, ISBN -13: 978-1-4051-1968-9.
[26] E.W. Washburn, The dynamics of capillary flow, Phys. Rev. 17 (3) (1921) 273–283.
[27] B. Vaziri Hassas, F. Karakas, M.S. Celik, Ultrafine coal dewatering: relationship between hydrophilic lipophilic balance (HLB) of surfactants and coal rankafine coal dewatering: relationship between hydrophilic lipophilic balance (HLB) of surfactants and coal rank, Int. J. Miner. Process. 133 (2014) 97–104, http://dx.doi.org/10.1016/j.minpro.2014.10.010.
[28] D. Hewitt, D. Fornasiero, J. Ralston, Bubble-particle attachment, J. Chem. Soc. Faraday Trans. 91 (13) (1995) 1997–2001, http://dx.doi.org/10.1039/FT9959101997.
[29] Z. Dai, D. Fornasiero, J. Ralston, Particle-bubble attachment in mineral flotation, J. Colloid Interface Sci. 217 (1999) 70–76, http://dx.doi.org/10.1006/jcis.1999.6319.
[30] B. Pyke, D. Fornasiero, J. Ralston, Bubble-particle heterocoagulation under turbulent conditions, J. Colloid Interface Sci. 265 (2003) 141–151, http://dx.doi.org/10.1016/s0021-9797(03) 00345-x.
[31] J. Duan, J. Fornasiero, J. Ralston, Calculation of the flotation rate constant of chalcopyrite particles in an ore, Int. J. Miner. Process. 72 (2003) 227–237.
[32] G.S. Dobby, J.A. Finch, Particle size dependence in flotation derived from a fundamental model of the capture process, Int. J. Miner. Process. 27 (1987) 241–263.
[33] R. Crawford, J. Ralston, The influence of particle size and contact angle in mineral flotation, Int. J. Miner. Process. 23 (1988) 1–24.
[34] A.V. Nguyen, J. Ralston, H.J. Schulze, On modeling of bubble-particle attachment probability in flotation, Int. J. Miner. Process. 53 (1998) 225–249, http://dx.doi.org/10.1016/s0301-7516(97) 00073-2.
[35] S., Kouachi, A., Hassanzadeh, M., Bouhenguel, B., Vaziri Hassas, M.S., Celik, 2015, Contribution of interceptional effect to collision efficiency of particle bubble encounter in flotation, XVI Balkan Mineral Processing Congress, 17–19 June 2015, Belgrade-Serbia.
[36] H.J. Schulze, Hydrodynamics of bubble-mineral particle collisions, Miner.Process. Extr. Metall. Rev. 5 (1989) 43–76.

[37] Z. Dai, S. Dukhin, D. Fornasiero, J. Ralston, The inertial hydrodynamic interaction of particles and rising bubbles with mobile surfaces, J. Colloid Interface Sci. (1998) 275–292.
[38] S. Kouachi, M. Bouhenguel, A. Amirech, A. Bouchemma, Yoon-Luttrell collision and attachment models analysis in flotation and their application on general flotation kinetic model, Desalination 264 (2010) 228–235, http://dx.doi.org/10.1016/j.desal.2010.06.057.
[39] D.I. Verrelli, W.J. Bruckard, P.T.L. Koh, M.P. Schwarz, B. Follink, Particle shape effect in flotation. Part 1: microscale experimental observations, Miner. Eng. 58 (2014) 80–89, http://dx.doi.org/10.1016/j.mineng.2014.01.004.
[40] J. Ralston, S.S. Dukhin, N.A. Mishchuk, Inertial hydrodynamic particle-bubble interaction in flotation, Int. J. Miner. Process. 56 (1999) 207–256, http://dx.doi.org/10.1016/s0301-7516(98) 00049-0.
[41] Z. Brabcova, T. Karapantsios, M. Kostoglou, P. Basarova, K. Matis, Bubble-particle collision interaction in flotation systems, Colloids Surf. A: Physicochem. Eng. Aspects 473 (2015) 95–103.
[42] C.M. Phan, A.V. Nguyen, J.D. Miller, G.M. Evans, G.J. Jameson, Investigation of bubble-particle interactions, Int. J. Miner. Process. 72 (2003) 239–254, http://dx.doi.org/10.1016/s0301-7516(03) 00102-9.
[43] B. Shahbazi, B. Rezai, S.M.J. Koleini, Bubble–particle collision and attachment probability on fine particles flotation, Chem. Eng. Process. 49 (2010) 622–627.
[44] J.P. Anfruns, J.A. Kitchener, The absolute rate of capture of single particles by single bubbles, in: M.C. Fuerstenau (Ed.), Flotation—A.M. Gaudin Memorial Volume, vol. 2, Society Mineral Engineers (SME), 1976, pp. 625–637.
[45] D.I. Verrelli, P.T.L. Koh, A.V. Nguyen, Particle-bubble interaction and attachment in flotation, Chem. Eng. Sci. 66 (2011) 2910–2921.
[46] D.I. Verrelli, B. Albijanic, A comparison of methods for measuring the induction time for bubble-particle attachment, Miner. Eng. 80 (2015) 8–13, http://dx.doi.org/10.1016/j.mineng.2015.06.011.
[47] O. Ozdemir, C. Karaguzel, A.V. Nguyen, M.S. Celik, J.D. Miller, Contact angle and bubble attachment studies in the flotation of trona and other soluble carbonate salts, Miner. Eng. 22 (2) (2009) 168–175.
[48] I. Bibi, B. Singh, E. Silvester, Dissolution of illite in saline-acidic solution at 25 °C, Geochemica et Cosmochemica Acta 75 (2011) 3237–3249.
[49] B., Mutaftschiev, 1982, Interfacial aspects of phase transformations, NATO Advanced Study Institute Series, vol. 87, pp. 63-102, ISBN: 978-94-009-7872-0, 10.1007/978-94-009-7870-6.
[50] F., Karakas, B., Vaziri Hassas, 2015, Effect of surface roughness on interaction of particles in flotation, Physicochemical problems of mineral processing, vol. 52(1), 2016, 19–35, 10.5277/ppmp150302.
[51] B., Vaziri Hassas, F., Karakas, O., Guven, M.S., Celik, 2014 (2), Effect of hydrophilic lipophilic balance (HLB) of nonionic surfactants on ultrafine lignite dewatering, XXVII International Mineral Processing Congress, Santiago—Chile.
[52] A. Vidyadhar, K. Hanumantha Rao, I.V. Chernyshova, Pradip, Forssberg, KSE, Mechanisms of amine–quartz interation in the absence and presence of alcohols studied by spectroscopic methods, J. Colloid Interface Sci. 256 (2001) 59–72.
[53] R.N. Wenzel, Resistance of solid surfaces to wetting by water, Ind. Eng. Chem. 28 (8) (1936) 988–994, http://dx.doi.org/10.1021/ie50320a024.
[54] A.B.D. Cassie, S. Baxter, Wettability of porous surfaces, Trans. Faraday Soc. 40 (1944) 546, http://dx.doi.org/10.1039/tf9444000546.
[55] A.B.D. Cassie, Contact angles, Trans. Faraday Soc. 3 (1948) 11, http://dx.doi.org/10.1039/df9480300011.
[56] L. Gao, T.J. McCarthy, How Wenzel and Cassie were wrong, Langmuir 23 (2007) 3762–3765, http://dx.doi.org/10.1021/la062634a.
[57] L. Gao, T.J. McCarthy, An attempt to correct the faulty intuition perpetuated by the wenzel and cassie laws (letter), Langmuir 25 (13) (2009) 7249–7255.
[58] H.J. Busscher, A.W.J. van Pelt, P. de Boer, H.P. de Jong, J. Arends, The effect of surface roughening of polymers on measured contact angles of liquids, Colloids Surf. 9 (1984) 319–331, http://dx.doi.org/10.1016/0166-6622(84) 80175-4.
[59] T.T. Chau, W.J. Bruckard, P.T.L. Koh, A.V. Nguyen, A review of factors that affect contact angle and implications for flotation practice, Adv. Colloid Interface Sci. 150 (2009) 106–115, http://dx.doi.org/10.1016/j.cis.2009.07.003.
[60] R.E. Johnson, R.H. Dettre, Contact angle hysteresis, advances in chemistry series, Am. Chem. Soc. 43 (1964) 112–135.
[61] J.D. Miller, S. Veeramasuneni, J. Drelich, M.R. Yalamanchili, G. Yamauchi, Effect of roughness as determined by atomic force microscopy on the wetting properties of PTFE thin films, Polym. Eng. Sci. 36 (14) (1996) 1849–1855.
[62] T. Dang-Vu, J. Hupka, J. Drzymala, Impact of roughness on hydrophobicity of particles measured by the washburn method, Physicochem. Prob. Miner. Process. 40 (2006) (2006) 45–52.
[63] J.W. Drelich, J.D. Miller, R.J. Good, The effect of drop (bubble) size on advancing and receding contact angle for heterogeneous and rough solid surfaces as observed with sessile-drop and captive-bubble techniques, J. Colloid Interface Sci. 179 (1996) 37–50, http://dx.doi.org/10.1006/jcis.1996.0186.
[64] J.W.G. Tyrrell, P. Attard, Atomic force microscope images of nanobubles on a hydrophobic surface and corresponding force-separation data, Langmuir 18 (1) (2002) 160–167, http://dx.doi.org/10.1021/la0111957.
[65] L.A.C. Luderitz, An AFM Study of the Interactions Between Colloidal Particles (M.Sc. Dissertation), Technical University of Berlin, 2012.
[66] D.I., Verrelli, W.J., Bruckard, P.T.L., Koh, M.P., Schwarz, B., Follink, 2012. Influence of particle shape and roughness on the induction period for particle-bubble attachment, XXVI International Mineral Processing Congress, New Delhi—India.
[67] A. Gul, Separation of microlite from zircon by flotation, Can. Metall. Q. 45 (1) (2006) 111–116.
[68] G.S. Dobby, J.A. Finch, A model of particle sliding time for flotation size bubbles, J. Colloid Interface Sci. 109 (2) (1986) 493–498.
[69] G.H. Luttrell, R.H. Yoon, A hydrodynamic model for bubble-particle attachment, J. Colloid Interface Sci. 154 (1992) 129–137.
[70] J. Zawala, J. Drzymala, K. Malysa, An investigation into the mechanism of the three-phase contact formation at fluorite surface by colliding bubble, Int. J. Miner. Process. 88 (2008) 72–79.
[71] R.H. Yoon, J.L. Yordan, Induction time measurements for the quartz-amine flotation system, J. Colloid Interface Sci. 141 (2) (1991) 374–383.
[72] B. Albijanic, O. Ozdemir, A.V. Nguyen, D. Bradshaw, A review of induction and attachment times of wetting thin films between air bubbles and particles and its relevance in the separation of particles by flotation, Adv. Colloid Interface Sci. 159 (2010) 1–21.
[73] B. Albijanic, E. Amini, E. Wightman, O. Ozdemir, A.V. Nguyen, D.J. Bradshaw, A relationship between the bubble-particle attachment time and the mineralogy of a copper-sulphide ore, Miner. Eng. 24 (12) (2011) 1335–1339.